Progr Colloid Polym Sci (2004) 129: 9–15
DOI 10.1007/b100297

Tadashi Kato
Koji Minewaki
Kyoko Miyazaki
Youhei Kawabata
Toshiyuki Shikata
Shigeyuki Komura
Masatoshi Fujii

Effects of shear flow on structures of lamellar phase in a nonionic surfactant/water system

T. Kato (✉) · K. Minewaki · K. Miyazaki
Y. Kawabata · S. Komura · M. Fujii
Department of Chemistry,
Tokyo Metropolitan University, Hachioji,
Tokyo 192-0397, Japan
e-mail: kato-tadashi@c.metro-u.ac.jp

T. Shikata
Department of Macromolecular Science,
Osaka University, Toyonaka,
Osaka 560-0043, Japan

Abstract Effects of shear flow on the structure of a lamellar phase in $C_{16}E_7$ (hepta(oxyethylene glycol)-*n*-hexadecylether)/water system (40–55 wt% of $C_{16}E_7$) at 70 °C are studied by using small-angle neutron scattering (SANS), small-angle light scattering (SALS), and shear stress-shear rate relationships. The repeat distance takes a deep minimum (referred to as d^*) at the shear rate 0.1–1 s^{-1}. As the concentration of $C_{16}E_7$ decreases, the repeat distance at rest increases whereas d^* remains almost constant and nearly equal to the thickness of bilayers obtained from the line shape analysis of small angle X-ray scattering at rest. These results suggest that the water layer is excluded by shear flow and that the lamellar phase segregates into surfactant-rich and water-rich regions. Although macroscopic phase separation does not occur, SALS intensity takes a maximum at the shear rate giving d^*, which is consistent with the SANS results. Mechanism for the decrease in the repeat distance is discussed in relation to the change in the size of the lamellar domains.

Keywords Shear flow · Lamellar phase · Nonionic surfactant · Small angle scattering · SANS · SALS

Introduction

Structures of surfactant self-assemblies are often affected by shear flow because their characteristic relaxation time (τ) is usually long enough to satisfy the condition $\dot{\gamma}\tau > 1$ for the typical shear rate $\dot{\gamma} = 10^{-2} \sim 10^3\ s^{-1}$ [1]. In the past 10 years, effects of shear flow on the structure of the surfactant lamellar phase have been studied extensively by using microscopy, NMR, and various kinds of scattering techniques. After the pioneering work of Roux and coworkers [2–5] who found the transformation from the lamellar phase to the multilamellar vesicles (onions), various types of shear effects have been reported: change in orientation of membranes [6–8], sponge-to-lamellar transformation [9, 10], multilamellar-to-unilamellar vesicle transformation [11–13], reduction in the spacing [14–19], collapse of membranes [20], formation of multilamellar cylinders as intermediate structures between lamellar and onions [21–24], and formation of Ribbon phase [25]. These effects have been found for the shear rate of $1 \sim 5 \times 10^3\ s^{-1}$. In our previous studies, on the other hand, attention has been paid to the behaviors at relatively low shear rates, $10^{-3} \sim 50\ s^{-1}$. At these shear rates, we have measured small-angle neutron scattering (SANS) on the lamellar phase of a nonionic surfactant $C_{16}H_{33}(OC_2H_4)_7OH$ ($C_{16}E_7$)/D_2O system [15–17, 26]. This system was chosen because phase behaviors and structures of the micellar and lamellar phases had been studied extensively by us [27–30]. We have found that the repeat distance (d) decreases significantly (down to about 40% of the initial d value in the extreme case) and discontinuously by shear flow [26]. In the present study, to confirm these findings, we have measured small angle light scattering (SALS) and the shear stress as a function of shear rate, in addition to further analyses of the SANS data.

Experimental

Materials

$C_{16}E_7$ was purchased from Nikko Chemicals, Inc. in crystalline form (>98%) and used without further purification. Deuterium oxide purchased from ISOTEC, Inc. (99.9%) was used after being degassed by bubbling of nitrogen to avoid oxidation of the ethylene oxide group of surfactants. Samples containing the desired amount of surfactant and water (~10 g) were sealed in an Erlenmeyer flask. For homogenization, we annealed samples for 3 h at about 55 °C with occasional shaking and then held them at room temperature for 21 h. This treatment was repeated for about one week.

All the measurements were made at 70 °C because the existence region of the lamellar phase extends to the lower concentration above about 67 °C [27].

Shear SANS

Measurements of SANS were carried out at the instrument SANS-U of Institute for Solid State Physics of University of Tokyo in Tokai with a Couette-type shear cell. The cell consists of two concentric cylinders, an inner aluminum stator and an outer quartz rotor. The stator diameter and the gap are 48 and 1 mm, respectively. Details of the cell have been reported before [31].

The diameter of the neutron beam is 5 mm and the scattered neutrons are detected by a two dimensional position-sensitive detector having 65×65 cm^2 (128×128 pixels) area. The sample-to-detector distance is 1 m for all runs. Thus the momentum transfer is $0.3 < q < 2.5$ nm^{-1} ($q = (4\pi/\lambda)\ \sin\theta$, where 2θ is the scattering angle and $\lambda = 0.7$ nm is the neutron wavelength).

Two scattering configurations were used; one is the so-called radial configuration where the beam is directed through the center of the cell (along the velocity gradient direction), and the other is the tangential configuration where the beam is directed through the end of the cell (along the flow direction). The two-dimensional (2-D) SANS pattern in the flow-vorticity plane is obtained in the radial configuration, while that in the velocity gradient-vorticity plane is obtained in the tangential configuration. For the lamellar structure, there are three principal orientations, perpendicular, transverse, and parallel orientations, with the layer normal along the vorticity, flow, and velocity gradient directions, respectively. Therefore, the perpendicular and transverse orientations can be detected by using the radial configuration whereas the perpendicular and parallel orientations can be detected by using tangential configuration. It should be noted that in the tangential configuration the intensity for the vorticity direction is much lower than that for the velocity gradient direction even for an isotropic sample due to the path differences of the scattered neutron beam. So only the radial configuration is used for detecting the perpendicular orientation.

After we transferred the sample into the outer rotor, we put in the stator as slowly as possible at the temperature where isotropic phases exist, that is, 45 °C for the 48 wt % sample (bicontinuous cubic (V_1) phase) and 50 °C for the 40 wt% sample (micellar (L_1) phase). Then the sample was heated to 70 °C and held for about 20 min before the first collection of SANS data at rest. At each shear rate, SANS data were collected every 10 min first for either the radial or the tangential configuration for 1–3 h to detect the change in the structure as a function of time. After that, the scattering configuration was changed from the radial (tangential) to the tangential (radial) configuration and data collection was made in the last 20 min for each shear rate. Although a vapor seal is incorporated in our cell, it is difficult to keep the concentration of the sample over 8–9 h at 70 °C. Hence, two independent runs were necessary to cover the desired range of the shear rate.

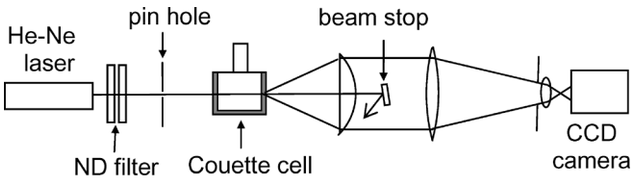

Fig. 1 Schematic representation of the shear SALS apparatus

Shear stress and shear SALS

A Rheometer (Nihon Rheology Kiki, NRM-2000) was modified for SALS measurements under shear flow. Figure 1 shows schematic representation of the apparatus. The light source is a He-Ne laser (NEC GLG5360, 5 mW at 632.8 nm). The sample cell is the same as that for SANS measurements except for that both stator and rotor are made of quartz. The temperature of the cell is controlled to ±0.1 °C by Peltier elements and a heater in an air bath. The intensity of scattered light is detected by a CCD camera system (Hamamatsu Photonics C4880-80-22A). Details of the apparatus will be reported elsewhere [32]. In the present study, measurements have been performed in unpolarized configuration; neither polarizer nor analyzer has been inserted in the optical path.

For the 55 wt% sample, shear stress has been measured with a cone-and-plate rheometer (Rheometrics, ARES). Cone angle and radius are 25 mm and 0.04 rad, respectively.

Results and discussion

Decrease in repeat distance

Figure 2 shows evolution of 1-D (one dimensional) SANS patterns in the velocity gradient direction of the tangential configuration (corresponding to the parallel orientation) obtained by integrating the scattering intensity over a segment of width $\Delta\phi = \pm 10°$ (ϕ: azimuthal angle) with increasing shear rate (at 48 wt%). These data were collected 1–3 h after the changing shear rate (see the experimental section) and so in almost stationary states except for the patterns (C) and (D) which were obtained 10 and 20 min after the changing the shear rate from 0.3 to 1 s^{-1}, respectively.

In Fig. 3, the repeat distance (d) obtained from the first reflection at 48 wt% is plotted against the shear rate. In the range 0–0.1 s^{-1}, the repeat distance depends on the shear rate only slightly. When the shear rate increases from 0.3 to 1 s^{-1}, the repeat distance decreases suddenly to 5.2 nm. With the further increase in the shear rate, d increases again through a minimum (referred to as d^*, hereafter). Figure 3 demonstrates that the shear rate dependence of d is almost the same for all the principal orientations of lamellae.

It can be seen from Fig. 2 that two separated peaks are observed 10 min after the changing shear rate from 0.3 to 1 s^{-1} (C). After 20 min, the peak at the lower angle disappears whereas the peak at the higher angle increases (D). The position of this peak remains unchanged even

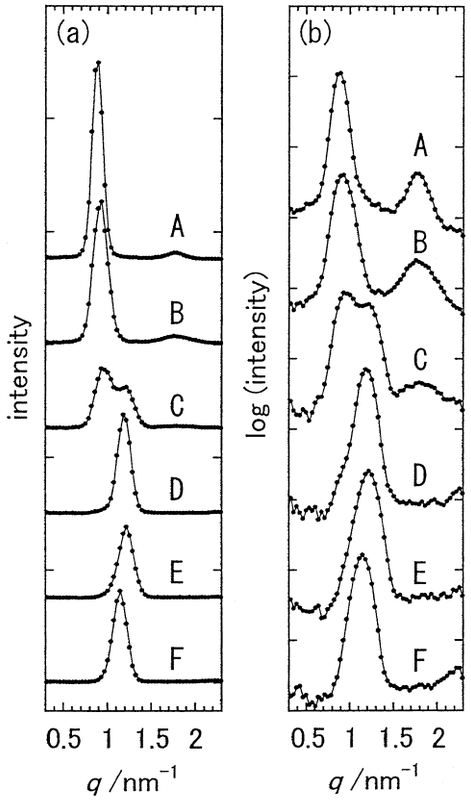

Fig. 2a,b Evolution of 1-D SANS patterns with increasing shear rate in the velocity gradient direction of the tangential configuration (corresponding to the parallel orientation) at 48 wt% obtained by integrating scattering intensity over a segment of width $\Delta\phi = \pm 10°$ where ϕ is the azimuthal angle [26]. The scattering intensities are represented in: **a** normal; **b** log scales. The patterns A, B, E, and F are obtained in the stationary state for the shear rate 0, 0.3, 1, and 3 s^{-1}, respectively. The patterns C and D are obtained 10 and 20 min after the changing shear rate from 0.3 to 1 s^{-1}, respectively

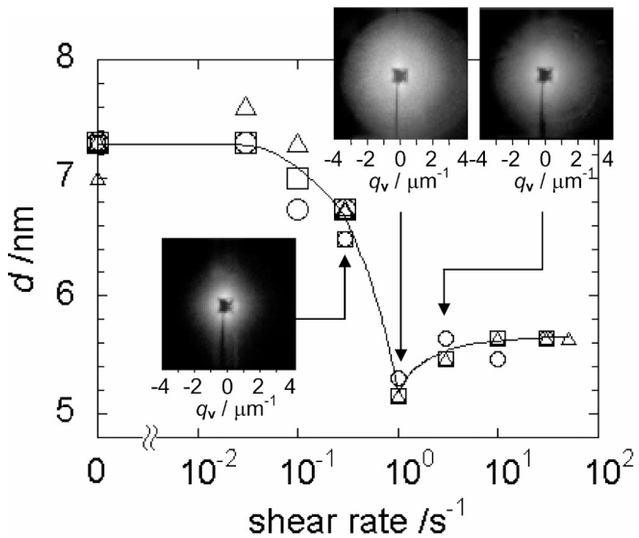

Fig. 3 Shear rate dependence of the repeat distance for the vorticity (*open circles*), transverse (*open squares*), and parallel (*open triangles*) orientations [26]. The different symbol sizes correspond to different runs (see the experimental section). Inserted images are 2-D SALS patterns for the shear rate 0.3, 1, and 3 s^{-1} from left to right

after 1 h, although the peak height decreases (E). These results indicate that the decrease in the repeat distance at 1 s^{-1}occurs discontinuously, suggesting some sort of transition. Similar shear rate dependence of the repeat distance has been observed for other concentrations except for the difference in the specific shear rate ($\dot{\gamma}^*$) giving d^*. At 40 and 55 wt%, $\dot{\gamma}^*$ is 0.1–0.3 s^{-1} which is slightly lower than that at 48 wt%. At present, however, it is difficult to discuss the concentration dependence of $\dot{\gamma}^*$ because it depends on shear history [16].

Figure 4 shows concentration dependence of the repeat distance at rest (d_0) and d^* (see the open symbols). As the concentration of $C_{16}E_7$ decreases from 55 to 40 wt%, d_0 increases from 6.5 nm to 8.5 nm whereas d^* is almost independent of concentration. At 40 wt%, the repeat distance decreases from 8.5 nm to 5.2–5.6 nm and so the amount of the reduction is fairly large compared to other two concentrations.

Exclusion of water layers

In a dilute lamellar phase formed by nonionic surfactant, the repulsive interactions between membranes are dominated by undulation fluctuations of membranes [33, 34]. In this case, the volume fraction of membrane (ϕ_s) can be expressed in terms of the repeat distance d as

$$d = \frac{2\delta A_s}{\phi_s A_\perp} \tag{1}$$

where δ is the half-thickness of membranes, A_s is the total membrane area, and $A_\perp$ is the membrane area projected on the plane orthogonal to the mean membrane normal. It has been shown from theoretical arguments that the shear flow suppresses undulation fluctuations of bilayers [35–39]. This leads to a reduction in the ratio $A_s/A_\perp$ and therefore in the repeat distance. In fact, the reduction of d by shear flow has been found experimentally [14, 18, 19]. In these studies, however, the ratio $(d_0–d)/d_0$ (d_0 and d are the repeat distance at rest and under shear, respectively) is only a few %. In the present study, on the other hand, $(d_0–d^*)/d_0$ is about 40, 30, and 25% at 40, 48, and 55 wt%, respectively. Such a large amount of reduction in the repeat distance has not been reported so far.

When the repeat distance decreases without a change of ϕ_s, Eq. (1) gives an expression of $(d_0–d)/d_0$ in terms of the membrane area as

$$\frac{d_0 - d}{d_0} = 1 - \frac{A_s/A_\perp}{A_{s0}/A_\perp} \tag{2}$$

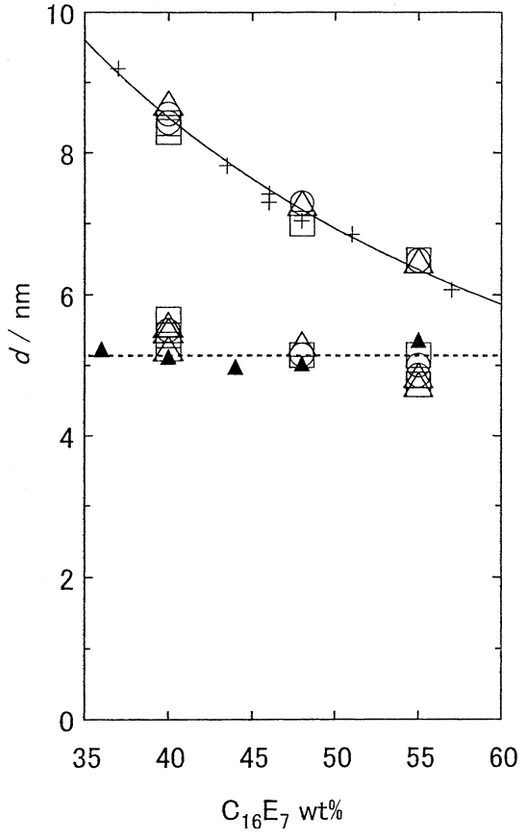

Fig. 4 Concentration dependence of the repeat distance at rest (*open symbols, upper*) and the minimum value under shear d^* (*open symbols, lower*), d^*, for the vorticity (*open circles*), transverse (*open squares*), and parallel (*open triangles*) orientations [26]. The *crosses* and *closed triangles* indicate the repeat distance and the total thickness of the bilayers, respectively, obtained from small-angle X-ray scattering at rest [27]

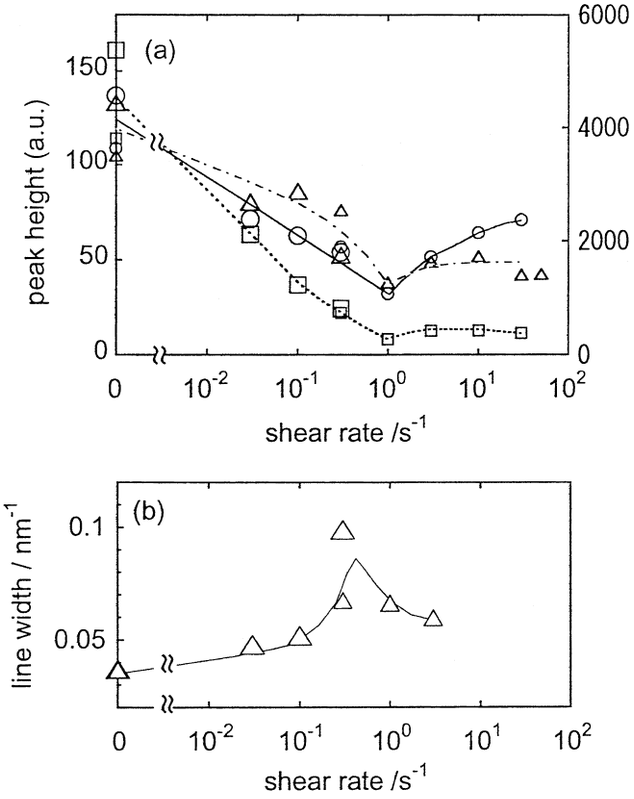

Fig. 5a,b Shear rate dependences of: **a** the peak height; **b** the line width of the first reflection for the vorticity (*open circles*), transverse (*open squares*), and parallel (*open triangles*) orientations. The different symbol sizes correspond to different runs. In part (a), the left ordinate indicates the peak height for the vorticity and transverse orientations whereas the right ordinate for the parallel orientation. The units of these axes are arbitrary. The intensity for the parallel orientation cannot be compared with those for the vorticity and the transverse orientations

where A_s and A_{s0} are the total membrane areas under shear and at rest, respectively. Because the relation $1 < A_s/A_\perp < A_{s0}/A_\perp$ holds, $(d_0–d)/d_0$ cannot exceed $(1–A_\perp/A_{s0})$ even if $A_s/A_\perp = 1$. In our previous study [27], we have studied the structure of the lamellar phase at rest formed in the same system ($C_{16}E_7$–D_2O) using small-angle X-ray scattering (SAXS). It has been found that d is inversely proportional to ϕ_s above 70 °C, which indicates that $A_\perp/A_{s0}$ is close to unity. This, together with the foregoing relation $(d_0–d)/d_0 < (1–A_\perp/A_{s0})$, indicates that $(d_0–d)/d_0$ should be much smaller than unity. Thus, $(d_0–d^*)/d_0$ cannot be as large as in the present study without the change in the concentration.

In our previous study [27], we have also obtained the half-thickness of the hydrophobic layer δ_{hc} and the thickness of the hydrophilic layer δ_{eo} from the line shape analysis of SAXS. Figure 4 includes the total membrane thickness at rest (closed triangles) obtained from these data ($2\delta = 2\delta_{hc} + 2\delta_{eo}$) together with d_0 (closed circles). Interestingly, d^* is nearly equal to 2δ. It should be noted that the thickness may decrease slightly by shear flow [17]. Nevertheless, this result strongly suggests that the water layer in the lamellar phase is excluded by shear flow, leading to segregation into water-rich and surfactant-rich regions. During the shear SANS measurements, however, we could not observe any turbidity of the sample to the naked eye. So we may infer that the segregated regions do not reach macroscopic size.

Figure 3 also includes 2-D SALS patterns at different shear rates at 48 wt%. The light scattering intensity increases substantially as the shear rate increases from 0.3 to 1 s^{-1}. As the shear rate increases further, the scattering intensity decreases but still larger than that at 0.3 s^{-1}. When the surfactant-rich and water-rich regions coexist, the difference in the concentration between these regions should increase with the decrease in the repeat distance in the lamellar (surfactant-rich) region. Because the light scattering intensity is proportional to the magnitude of concentration fluctuations, the light

scattering intensity is expected to take a maximum at $\dot{\gamma} = \dot{\gamma}^*$. Thus, the SALS results are consistent with the SANS results.

Bruinsma and Rabin [36] predicted that such a shear-induced segregation occurs above a critical shear rate given by

$$\dot{\gamma}_c \cong \frac{(k_B T)^{5/2}}{\eta \kappa^{3/2} d^3} = \frac{k_B T}{\eta (\kappa / k_B T)^{3/2} d^3} \tag{3}$$

where k_B is the Boltzmann constant, T the absolute temperature, η the viscosity of solvent, κ the bending constant of a surfactant layer, and d the interlayer spacing. For $\eta \sim 10^{-2}$ poise $= 10^{-3}$ Pa s, $d \sim 10$ nm, and $\kappa \sim k_B T$, $\dot{\gamma}_c$ is calculated to be 4×10^6 s^{-1} which is more than six orders of magnitude higher than $\dot{\gamma}^*$ in the present study. A fit to the observed $\dot{\gamma}^*$ (~ 1 s^{-1}) requires replacement of d by 1 μm or replacement of η by 10^4 poise $= 10^3$ Pa s. Ramaswamy [37] has also shown that the lamellar phase loses its stability and segregates above the critical shear rate given by the similar equation as Eq. (3). It should be noted that these theories assume direct suppression of undulation fluctuations of membranes by shear flow. In this case, the reduction of d should be observed only in the limited orientation. In the present study, however, the shear rate dependences of d are almost the same for all the principal directions as can be seen from Fig. 3.

Shear flow and lamellar domains

As described in the previous section, the present results cannot be explained by the existing theories. To find some clue as to how the shear flow affects the repeat distance, we compare the shear rate dependence of the repeat distance with other properties. Figure 5a shows the shear rate dependence of the peak heights for the three principal orientations obtained from the 1-D SANS pattern. Note that the peak heights for the vorticity and the transverse orientations are obtained from the radial configuration whereas the peak height for the parallel orientation is obtained from the tangential configuration. So the peak height for the parallel orientation cannot be compared with those for the perpendicular and transverse orientations. Figures 3 and 5a demonstrate that the peak height decreases significantly as the shear rate increases up to 0.1 s^{-1} where the jumping of the repeat distance does not yet occur. It has been known that the shear flow affects the orientation of lamellae [6–8]. If there is alignment, there should be an increase in the peak height in one direction (corresponding to that particular lamellar orientation) on the cost of the two others. In our experiments, however, the reduction of the peak height is observed for all the principal orientations, which cannot be explained by the change in the orientation of lamellae alone.

As can be seen from Fig. 2, the reduction of the peak height accompanies broadening of the line width. So we have obtained the line width from the least-square fitting of the 1-D SANS pattern for the parallel orientation to Gaussian distribution function given by

$$I(q) \propto \exp[-\frac{(q - q_0)^2}{2\sigma^2}] \tag{4}$$

where q_0 is the location of the first diffraction peak. If the resolution function and the scattering function are also Gaussian, σ can be expressed as $\sigma^2 = {\sigma_r}^2 + {\sigma_s}^2$ where σ_r and σ_s are the widths of the resolution function and the scattering function, respectively. Figure 5b shows shear rate dependence of σ_s obtained from σ and σ_r where σ_r is calculated from the following equation [40]:

$$\sigma_r^2 = \left(\frac{2\pi}{\lambda}\right)^2 \frac{d_b^2}{16L^2} + \left(\frac{2\pi}{\lambda}\right)^2 \frac{\Delta_D^2}{6L^2} + \frac{q_0^2}{6}\left(\frac{\Delta\lambda}{\lambda}\right)^2 \tag{5}$$

where λ and d_b are the wave length and the diameter of the neutron beam, L is the sample-to-detector length, Δ_D is the full width at half-maximum of the spatial resolution of the detector, and $\Delta\lambda$ is the width of the wave-length distribution. It can be seen from Fig. 5b that the line width σ_s increases with increasing shear rate up to 0.3 or 1 s^{-1} and, then, decreases. It has been known that broadening of the diffraction line is observed when the grain size (or domain size for the liquid crystal phase) decreases less than the critical value [41]. So the results in Fig. 5b may suggest that the lamellar domains are substantially shrunk by shear flow for the shear rate of 10^{-2} to 1 s^{-1}.

When we discuss the undulation fluctuations of membranes in the lamellar phase, it is tacitly assumed that the size of the lamellar domains (L_d) is much larger than the so-called ''patch'' or ''collision'' length (L_p) which dominates the repeat distance [42]. If the lamellar domains shrink so greatly as the condition $L_d >> L_p$ no longer holds, however, the mean amplitude of undulation fluctuations decreases significantly and so the lamellar spacing cannot be maintained. This can explain why the reduction of d occurs for the shear rate as low as 0.1 to 1 s^{-1}; the time scale of the fluctuation of the lamellar domain is expected to be much slower than of the undulation fluctuations of membranes. It should be noted, however, that σ_s is affected by not only the domain size but also the fluctuations of the repeat distance due to the undulation mode and/or the peristatic mode [43]. So we need analyses of the whole scattering curve taking into account these fluctuations as well as the domain size.

Finally, shear stress-shear rate relationships are shown in Fig. 6. For the 55 wt% sample, the shear stress slightly decreases with increasing shear rate between 2×10^{-2} and 5×10^{-1} s^{-1}. At 48 wt%, such behaviors may be seen in the shear rate range less than 2×10^{-2} s^{-1}. Note that these

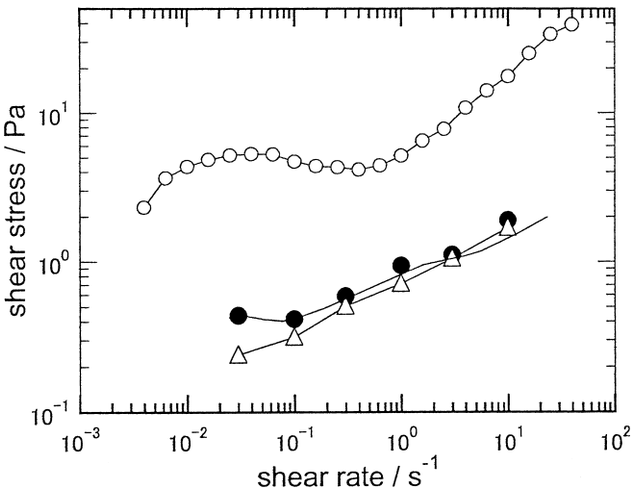

Fig. 6 Shear stress-shear rate relationships at 48 wt% (*closed circles*) and 55 wt% (*open circles*) obtained within 10 min after changing shear rate and that for the stationary state at 48 wt% (*triangles*)

results have been obtained within 10 min after changing the shear rate. The shear stress for the stationary state at 48 wt% show only monotonous increase (see the triangles). The result for the 55 wt% sample reminds us the theoretical prediction by Olmsted [44, 45] for phase separation at common stress or common strain rate (shear rate) for the shear thinning transition. However, such shear thinning behaviors can also be explained by the shrink of the lamellar domain. For further quantitative discussion, more systematic measurements of the shear stress are necessary. Work along this line is in progress and will be reported elsewhere.

Conclusions

The present results may be summarized as follows:

1. As the shear rate increases, the repeat distance (d) decreases discontinuously (down to ~40% of d at rest in the extreme case) at $0.1 \times 1\ s^{-1}$ and takes a minimum.
2. The shear rate dependences of d are almost the same for the three principal orientations of lamellae.
3. The minimum value of d (d^*) is almost independent of the concentration and nearly equal to the total thickness of bilayers at rest obtained from SAXS.
4. These results 1–3 suggest the shear-induced segregation into surfactant-rich and water-rich regions.
5. Although macroscopic phase separation does not occur, SALS intensity takes a maximum around the shear rate giving d^*, which is consistent with the SANS results.
6. The forgoing results cannot be explained by the existing theories. The shear rate dependences of the peak height and line width of the first reflection suggest that the shrink of the lamellar domain is correlated with the decrease in the repeat distance.

Acknowledgment This research was partially supported by Ministry of Education, Science, Sports and Culture, Grant-in-Aid for Scientific Research (B), 11440207, 1999, and 15340140, 2003.

References

1. For example, Pine, D (2000) In: Cates M, Evans MR, Osborne P (eds) Nonequilibrium dynamics, metastability and flow. Institute of Physics Publishing, Bristol, chap 2
2. Roux D (2000) In: Cates M, Evans MR, Osborne P (eds) Nonequilibrium dynamics, metastability and flow. Institute of Physics Publishing, Bristol, chap 7
3. Diat O, Roux D, Nallet F (1993) J Phys II France 3:1427
4. Diat O, Roux D, Nallet F (1995) Phys Rev E 51:3296
5. Sierro P, Roux D (1997) Phys Rev Lett 78:1496
6. Penfold J, Staples E, Lodhi AK, Tucker I, Tiddy GJT (1997) J Phys Chem B 101:66
7. Berghausen J, Zipfel J, Berghausen J, Lindner P, Richtering W (1998) Europhys Lett 43:683
8. Zipfel J, Berghausen J, Lindner P, Richtering W (1999) J Phys Chem B 103:2841
9. Yamamoto J, Tanaka H (1996) Phys Rev Lett 77:4390
10. Leon A, Bonn D, Meunier J, Al-Kahwaji A, Kellay H (2001) Phys Rev Lett 86:938
11. Bergmeier M, Gradzielski M, Hoffmann H, Mortensen K (1998) J Phys Chem B 102:2837
12. Bergmeier M, Gradzielski M, Hoffmann H, Mortensen K (1999) J Phys Chem B 103:1605
13. Hoffmann H, Bergmeier M, Gradzielski M, Thunig C (1998) Prog Colloid Polym Sci 109:13
14. Yamamoto J, Tanaka H (1995) Phys Rev Lett 74:932
15. Minewaki K, Kato T, Yoshida H, Imai M (1999) J Therm Anal Calorim 57:753
16. Minewaki K, Kato T, Imai M (2001) Stud Surf Sci Catal 132:185
17. Imai M, Nakaya K, Kato T (2001) Eur Phys J E 5:391
18. Idziak SHJ, Welch SE, Kisilak M, Mugford C, Potvin G, Veldhuis L, Sirota WB (2001) Eur Phys J E 6:139
19. Welch SE, Stezer MR, Hu G, Sirota EB, Idziak SH (2002) Phys Rev E 65:061511
20. Al-Kahwaji A, Kellay H (2000) Phys Rev Lett 84:3073
21. Weigel, Lauger J, Richtering W, Lindner P (1999) J Phys II France 6:529
22. Zipfel J, Nettesheim F, Lindner P, Le TD, Olsson U, Richtering W (2001) Europhys Lett 53:335
23. Le TD, Olsson U, Mortensen K, Zipfel J, Richtering W (2001) Langmuir 17:999

24. Nettesheim F, Zipfel J, Olsson U, Renth F, Linder P, Richtering W (2003) Langmuir 19:3618
25. Cristobal G, Rouch J, Panniza P, Narayanan T (2001) Phys Rev E 64:011505
26. Kato T, Minewaki K, Kawabata Y, Imai M, Takahashi Y (2004) Langmuir 20:3504
27. Minewaki K, Kato T, Yoshida H, Imai M, Ito K (2001) Langmuir 17:1864
28. Kato T, Taguchi N, Terao T, Seimiya T (1995) Langmuir 11:4661
29. Kato T, Taguchi N, Nozu D (1997) Progr Colloid Polym Sci 106:57
30. Kato T (2003) In: Esumi K, Ueno M (eds) Structure-performance relationships. Surfactants, 2nd edn. Marcel Dekker, New York, chap 11
31. Takahashi Y, Noda M, Naruse M, Kanaya T, Watanabe H, Kato T, Imai M, Matsushita Y (2002) J Soc Rheol Jpn 28:187
32. Miyazaki K, Minewaki K, Kawabata Y, Kato T (to be published)
33. Helfrich W (1978) Naturforsch 33a:305
34. Helfrich W (1985) J Phys (Paris) 46:1263
35. Cates ME, Milner ST (1989) Phys Rev Lett 62:1856
36. Bruinsma RF, Rabin Y (1992) Phys Rev A 45:994
37. Ramaswamy S (1992) Phys Rev Lett 69:112
38. Zilman AG, Granek R (1999) Eur Phys J B 11:593
39. Mallow S, Olmsted PD (2002) Eur Phys J E 8:485
40. Glinka CJ, Rowe JM, LaRock JG (1986) J Appl Crystallogr 19:427
41. Culity BD (1978) Element of X-ray diffraction. Addison-Wesley, Reading, MA
42. For example, Golubovic L, Lubensky TC (1999) Phys Rev B 39:12110
43. For example, Gelbart WM, Ben-Shaul A, Roux D (eds) (1994) Micelles, membranes, microemulsions, and monolayers. Springer, Berlin Heidelberg New York
44. Olmsted PD (1999) Europhys Lett 48:339
45. Fielding SM, Olmsted PD (2003) Phys Rev Lett 90:224501